Effect of cadmium sulfide nanorod content on Freedericksz threshold voltage, splay and bend elastic constants in liquid-crystal nanocomposites

2012 J. Phys. D: Appl. Phys. 45 235303

(http://iopscience.iop.org/0022-3727/45/23/235303)

IOP PUBLISHING JOURNAL OF PHYSICS D: APPLIED PHYSICS

J. Phys. D: Appl. Phys. **45** (2012) 235303 (9pp) doi:10.1088/0022-3727/45/23/235303

Effect of cadmium sulfide nanorod content on Freedericksz threshold voltage, splay and bend elastic constants in liquid-crystal nanocomposites

Prasenjit Nayek[1], Santanu Karan[2], Sudarshan Kundu[1], Seung Hee Lee[1], Sudeshna Das Gupta[3], Soumen Kumar Roy[4] and Subir Kumar Roy[2]

[1] Department of BIN Fusion Technology, Chonbuk National University, Jeonju, Jeonbuk, Jeonbuk 561-756, South Korea
[2] Department of Spectroscopy, Indian Association for the Cultivation of Science, Jadavpur, Kolkata-700032, India
[3] Lady Brabourne College, Department of Physics, Kolkata, India
[4] Department of Physics, Jadavpur University, Kolkata-700032, India

E-mail: spskr@iacs.res.in, spsk73@gmail.com and jitnayek@gmail.com

Received 16 February 2012, in final form 14 April 2012
Published 25 May 2012
Online at stacks.iop.org/JPhysD/45/235303

Abstract

This report describes how doping liquid crystals (LC) with rod-like hexagonal semiconductor nanoprisms alters the dielectric and elastic properties of the composites as compared with a pristine nematic liquid crystal (NLC). Cadmium sulfide nanorods were synthesized *via* the solvothermal process and blended with a NLC. Nanorods were highly miscible with NLC and produced a topological defect-free texture up to a certain limit. A good dark state was achieved during the homeotropic configuration of the cell within that limit. Appreciable changes in splay and bend elastic constants of the LCs were observed after blending with nanorods. Long-range order was established in the hybrid system, and consequently the anisotropy was increased. The threshold voltage decreased dramatically by ∼31%. Dielectric study revealed a high-frequency mode, which might be due to anchoring of the LC with nanorods.

(Some figures may appear in colour only in the online journal)

1. Introduction

Liquid-crystal display devices are propitious and astounding for modern life because of the ubiquity of their applications from wrist-watch to three-dimensional displays. Control over the long-range orientational order of the liquid crystal (LC) is critical for obtaining superior optical switching and display-device performance [1–7]. One of the superior approaches of achieving long-range order is to disperse anisotropic nanomaterials into an LC as an active matrix component. For incorporation of nanomaterials in an LC matrix, the proper selection of size, shape and crystallographic structure of the nanomaterials is crucial for boosting the performance of the device. For example, zero-dimensional particles or centro-symmetric materials are less responsive to external fields, and tend not to form long-range ordered structures. On the other hand, elongated anisotropic nanomaterials possessing an inherent permanent dipole moment respond dramatically in an applied field, facilitating alignment along the direction of the field [8, 9]. By choosing appropriate synthesis routes, inorganic nanocrystals have been tuned with an impressive variety of sizes and shapes [10–13]. Incorporation of nanomaterials into an LC matrix gives rise to the formation of topological defects due to deformations of the director (n) field around the surface of the incorporated colloid species, which breaks the continuous symmetry of the blend [6, 14–17]. Topological defects become more serious with impregnation of materials of larger dimensions and use of higher concentrations. Despite the fact that rod-like inclusions in nematics have been extensively studied for several decades,

both theoretically and experimentally [18–20], recently it has been demonstrated that altering the shapes of particles can lead to marked changes in the symmetry of their elastic interactions and the resulting colloidal assemblies in nematic liquid crystals (NLCs) [21–25]. Although the change in electro-optic responses due to the addition of inorganic non-mesogenic anisotropic nanoparticles in a NLC host has been shown and explained in some recent works [26, 27], studies of dielectric behaviour and change in elastic constants have not been conducted so extensively. The aim of this work is to study the dielectric and elastic constants of CdS nanorod NLC blends. Dielectric strength, relaxation frequency, polarizing optical microscopy and also splay and bend elastic constants were studied extensively.

2. Experimental

For the preparation of CdS nanorods 100mM of cadmium nitrate ($Cd(NO_3)_2 \cdot 4H_2O$) and 300mM thiourea (NH_2CSNH_2) were dissolved in a teflon-lined stainless steel autoclave filled up to 80% of its capacity with ethylenediamine. The autoclave was then heated at 200 °C for 12 h and then cooled to room temperature. The precipitate was centrifuged at 8000 rpm and washed several times with absolute ethanol. Finally, the powder of CdS NRs was obtained after drying in vacuum at 70 °C for 2 h. We first dissolved 2 mg CdS NRs in 20 ml chloroform and sonicated unless dissolved well, then took 1 ml mixture from the mother solution and added it to 9 ml chloroform, and taking 100 μl from the secondary solution in 100 ml NLC sonicated it for 10 min. Finally, by evaporating chloroform from the mixture we obtained a 0.001% CdS nanorod NLC blend (blend-1). Similarly, we prepared another 0.01% CdS NLC blend (blend-2). NLC was purchased from E. Merck. It is a blend of phenyl cyclohexanes, biphenyl cyclohexanes, cyanobiphenyls and cyclohexane carboxylates. The dielelectric anisotropy of the NLC blend is +11.4, optical anisotropy is 0.13, viscosity is 25 $mm^2\,s^{-1}$ at 20 °C. The pristine NLC shows transition from crystalline to the nematic phase at −5°C, whereas nematic to isotropic transition temperature T_{NI} is at 67°C. Sandwich-type planar pre-aligned empty cells (EHC) of thickness 10 μm and effective area of 16 mm^2 were used for the measurements. The cells were then filled at a temperature, a few degrees higher than their corresponding isotropic temperature, through the capillary action method. The filled cells were then cooled down slowly (1 °C min^{-1}) to 30 °C. A Mettler hot stage (FP82) was used for controlling the temperature of the cell with an accuracy of ±0.1 °C. For the automatic dielectric measurements in the frequency range from 5 Hz to 13 MHz, an impedance analyser (HP4192A) was used. A small number of CdS nanorods dissolved in chloroform and it was sonicated for 10 min. A few drops were taken on a glass plate and scanning electron microscopy (SEM) pictures were taken at different magnifications using field emission SEM (FESEM) (JSM-6700F, JEOL, JAPAN). Transmission electron microscopy (TEM) was performed with a JEM-2010, JEOL, Japan, transmission electron microscope. The specimens for the TEM measurements were prepared by depositing a drop of the dilute solution of the sample on a carbon-coated copper grid and drying at room temperature. A LEICA DMLP polarizing microscope was used for electro-optical studies. A CANNON digital camera interfaced with a computer was used for taking pictures of the textures for different bias voltages through a polarizing microscope. The dielectric measurements of the sample cell were preceded by the calibration of a similar cell with air and toluene. The frequency dependence of the imaginary part of dielectric permittivity was fitted with the extended Havriliak–Negami (HN) fit function, as given below:

$$\varepsilon'' = \frac{\sigma_0}{\varepsilon_0}.\frac{1}{\omega^s} + \sum_{k=1}^{N} \mathrm{Im}\left\{\frac{\Delta\varepsilon_k}{[1+(\mathrm{i}\omega\tau_k)^{\alpha_k}]^{\beta_k}}\right\}. \quad (1)$$

The characteristic dielectric strength, $\Delta\varepsilon_k$, relaxation frequency, $f_k = 1/2\pi\tau_k$, distribution parameter, α_k, and asymmetric parameter, β_k, of each individual process k involved in dielectric relaxation and the conduction parameter σ_0 are included in equation (1). The first term on the right-hand side of equation (1) describes the motion of free charge carriers in the sample, which contribute to the dc loss. In the case of an Ohmic behaviour ($s = 1$), σ_0 is the Ohmic conductivity of the NLC. The dielectric strength, $\Delta\varepsilon_k$, relaxation time, τ_k, and dc conductivity (σ_0) were extracted after fitting of the extended HN [28]. Other theoretical calculations were also performed in order to find the changes in elastic constants, and those are presented in the following section.

3. Results and discussion

Figure 1(*a*) shows the TEM images of ethylenediamine-coated CdS nanorods with an average diameter of 25–30 nm. The hexagonal crystal structure of the nanorod was confirmed from powder XRD patterns and the same are shown in figure 1(*b*). Figure 1(*c*) shows that the surface of the nanorods is mostly covered with ethylenediamine through the interaction of surface Cd^{2+} ions and plays a critical role in the growth of nanorods. Both monodentate and bridging interactions of surface Cd^{2+} ions with ethylenediamine are possible and may contribute to the dipole moment of the CdS nanorods as ethylenediamine has a net dipole moment of 1.8 D. The SEM image is shown in figure 2(*a*) and it shows the large-scale production of CdS nanorods. The length distribution of CdS nanorods from the FESEM picture is shown in figure 2(*b*). It is clear that maximum CdS nanorods have length ∼629 nm by fitting the statistical histogram using a Gaussian distribution function.

We have given a schematic view of the expected alignment of the director around the CdS nanorod during the field OFF and field ON states in figures 3(*a*) and (*b*), respectively. Here we have shown that $\hat{n}$ is the average director of NLCs and $\hat{z}$ is the axis of the CdS nanorod. Due to moderately strong/intermediate anchoring between them arrangement of the NLCs at the nanorod surface and far away from that will be completely different during the field OFF state, which is depicted in the schematic given in figure 3(*a*). Nevertheless, when an electric field is applied, the blend aligns along the direction of the field producing a global unidirectional

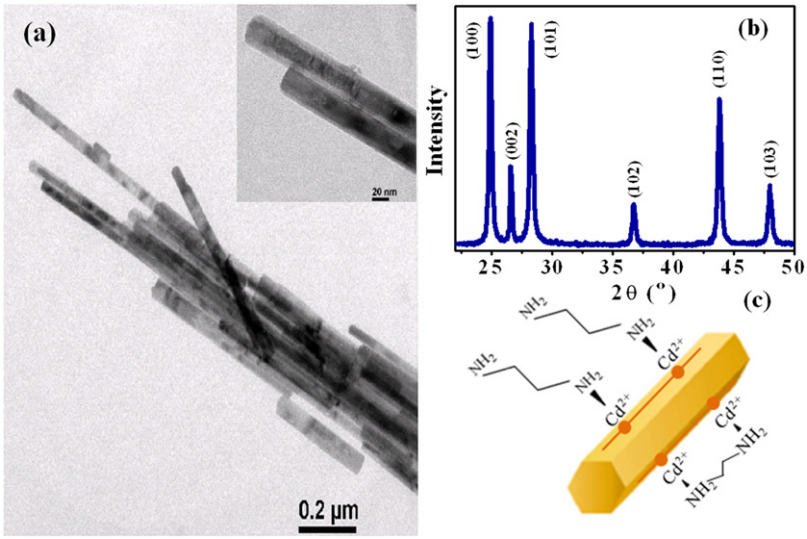

Figure 1. (*a*) TEM pictures of the CdS nanorods. The inset shows that the average diameters of the rods are 25–30 nm. (*b*) XRD pattern of the CdS nanorods with hexagonal crystal packing. (*c*) Scheme of a CdS nanorod with ethylenediamine attached on its surface.

orientation of the rods and LC directors, defining a unique axis for the system, which is shown schematically in figure 3(*b*).

The threshold voltage, the splay (K_{11}) and bend (K_{22}) elastic constants were extracted from the C–V curve (30 °C) shown in figure 4, by the method suggested by Morris *et al* [29].

K_{11} is related to the Freedericksz threshold [30] voltage, $V_{\rm th}$, by the relation

$$K_{11} = \frac{\varepsilon_0 \Delta\varepsilon}{\pi^2} V_{\rm th}^2 \tag{2}$$

where ε_0 is the permittivity of free space and $\Delta\varepsilon = \varepsilon_\parallel - \varepsilon_\perp$ is the dielectric anisotropy of the sample. The method of determination of $\Delta\varepsilon$ is described below:

Gruler *et al* [31] suggested that

$$\frac{V}{V_{\rm th}} = \frac{2}{\pi}(1+\gamma \sin^2\varphi_{\rm m})^{1/2} \times \int_0^{\varphi_{\rm m}} \left[\frac{(1+\kappa \sin^2\varphi)}{(1+\gamma \sin^2\varphi)(\sin^2\varphi_m - \sin^2\varphi)}\right]^{1/2} {\rm d}\varphi \tag{3}$$

and

$$\frac{C}{C_\perp} = \frac{\int_0^{\varphi_{\rm m}} \left[\frac{(1+\kappa \sin^2\varphi)(1+\gamma \sin^2\varphi)}{(\sin^2\varphi_{\rm m} - \sin^2\varphi)}\right]^{1/2} {\rm d}\varphi}{\int_0^{\varphi_{\rm m}} \left[\left[\frac{(1+\kappa \sin^2\varphi)}{(1+\gamma \sin^2\varphi)(\sin^2\varphi_{\rm m} - \sin^2\varphi)}\right]^{1/2} {\rm d}\varphi\right]} \tag{4}$$

where $\kappa = (K_{33}/K_{11}) - 1$ (K_{33} being the bend elastic constant), $\gamma = (\varepsilon_\parallel/\varepsilon_\perp) - 1$, φ is the tilt angle made by the director with a direction parallel to the cell walls, $\varphi_{\rm m}$ is the tilt angle at the centre of the cell, and $C_\perp$ is the capacitance of the cell when the LC molecules are homogeneously aligned, that is before the onset of Freedericksz transition when the voltage applied is lower than the threshold voltage. These equations can be combined to yield

$$\frac{C - C_\perp}{C_\perp} = \gamma - \frac{2\gamma}{\pi}(1+\gamma \sin^2\varphi_{\rm m})^{1/2}\frac{V_{\rm th}}{V} \times \int_0^{\sin\varphi_{\rm m}} \left[\frac{(1+\kappa x^2)(1-x^2)}{(1+\gamma x^2)(\sin^2\varphi_{\rm m} - x^2)}\right]^{1/2} {\rm d}x \tag{5}$$

when the applied voltage is much higher than the threshold voltage, the director at the centre of the cell becomes perpendicular to the cell walls and $\varphi_{\rm m} = \pi/2$, then the above equation reduces to

$$\frac{C - C_\perp}{C_\perp} = \gamma - \frac{2\gamma}{\pi}(1+\gamma)^{1/2}\frac{V_{\rm th}}{V}\int_0^1 \left[\frac{(1+\kappa x^2)}{(1+\gamma x^2)}\right]^{1/2} {\rm d}x \tag{6}$$

or dividing by γ,

$$\frac{C - C_\perp}{C_\parallel - C_\perp} = C_{\rm R} = 1 - \frac{2}{\pi}(1+\gamma)^{1/2}\frac{V_{\rm th}}{V} \times \int_0^1 \left[\frac{(1+\kappa x^2)}{(1+\gamma x^2)}\right]^{1/2} {\rm d}x \tag{7}$$

where $C_{\rm R}$ may be called the reduced capacitance. $C_\parallel$ is the capacitance of the cell when the nematic is homeotropically oriented, i.e. the value of C in the limit $1/V \to 0$. $\varepsilon_\parallel$ and $\varepsilon_\perp$ may be obtained by dividing $C_\parallel$ and $C_\perp$ by the empty cell capacitance C_0, respectively. In the above equation, the parameter γ represents $(C_\parallel - C_\perp)/C_\perp$. Equation (6) predicts that a plot of $(C_\parallel - C_\perp)/C_\perp$ against $1/V$ for $V \gg V_{\rm th}$ should be linear and the extrapolated value of the ordinate for $1/V \to 0$ should directly provide the value of $\gamma = \Delta\varepsilon/\varepsilon_\perp$. The variation of capacitance with applied voltage was fitted against equations (3) and (4) to obtain $V_{\rm th}$ and κ. We then used equation (2) to calculate K_{11} and hence K_{33} at 30 °C for all measurements. A two-parameter non-linear least-squares fit for finding $V_{\rm th}$ and κ ($(K_{33}/K_{11}) - 1$) worked out by starting with values of $V_{\rm th}$ and γ ($(\varepsilon_\parallel/\varepsilon_\perp) - 1$) taken directly from the experiment. Equation (3) was then used to obtain the $\varphi_{\rm m}$'s for all values of V for which measurements of capacitance were carried out. The $\varphi_{\rm m}$'s thus obtained were used in equation (4) to obtain C; the error that was minimized in the least-squares program was $\sum_{i=1}^{i=n} (C_i^{\rm expt} - C_i)^2$, where $C_i^{\rm expt}$ is the measured value of the capacitance at $V = V_i$ and C_i is the value of capacitance obtained by solving equation (4), n being the number of data points at a particular temperature. The final value of $V_{\rm th}$ never

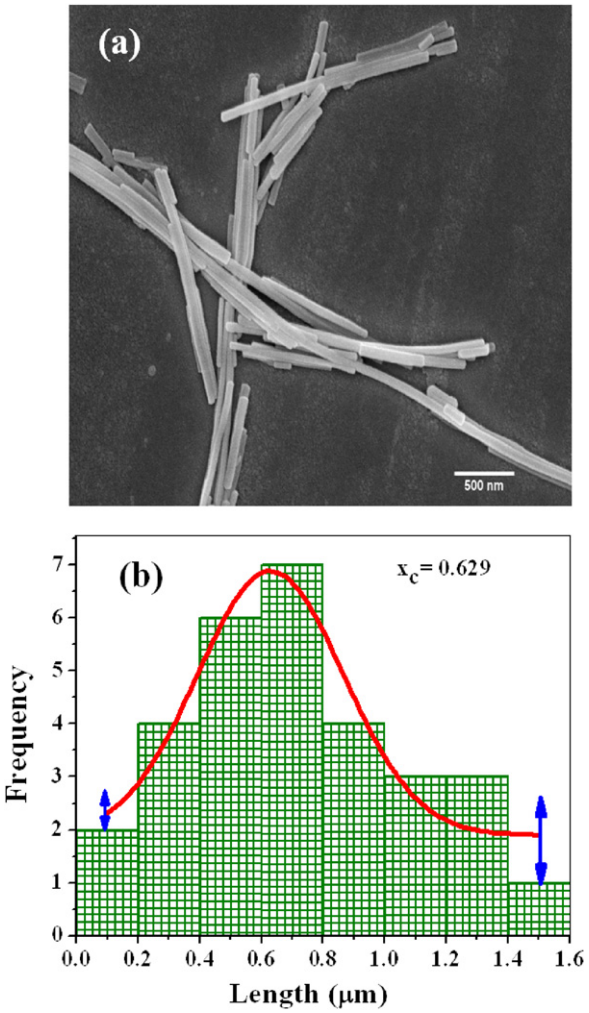

Figure 2. (*a*) SEM image; it shows the large-scale production of CdS nanorods. (*b*) Length distribution of the nanorods from the FESEM picture; it is clear that maximum CdS nanorods have length ∼629 nm by fitting the statistical histogram using a Gaussian distribution function: $y = y_o + (A/w\sqrt{\pi/2})e^{-2((x-x_c)^2/w^2)}$, where y_0 is the offset, x_c is the mean (location of the peak), w is the width and A is the area of the curve.

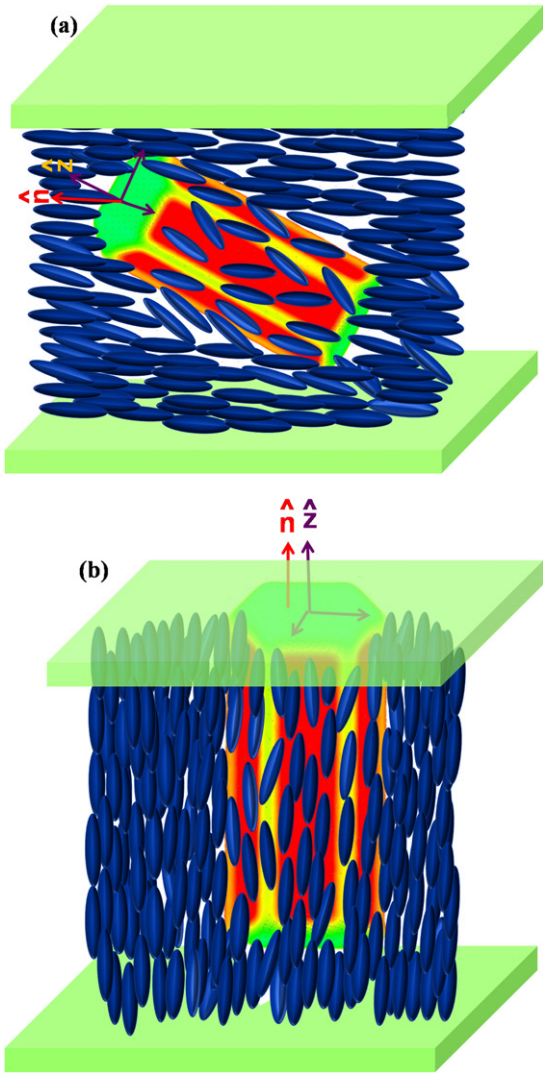

Figure 3. Schematic diagram showing (*a*) arrangement of the NLCs surrounding the nanorod under the field OFF condition. The director for NLC and long axis of nanorod are not exactly the same and the NLCs at the surface of the nanorods are not similar with respect to the NLCs far away from the nanorod walls. (*b*) Global alignment of the NLCs and nanorod uniaxially under the electric field ON state.

differed to a great extent from the input values. Splay (K_{11}) and bend (K_{33}) elastic constants are the important parameters in LC display devices and we calculated those constants from the C–V curve (30 °C) by the method suggested by Morris *et al*. A two-parameter non-linear least-squares fit for finding V_{th} and κ $((K_{33}/K_{11}) - 1)$ worked out by starting with values of V_{th} and γ $((\varepsilon_\parallel/\varepsilon_\perp) - 1)$ which were taken directly from the experiment. The error that was minimized in the least-squares program is $\sum_{i=1}^{i=n}(C_i^{expt} - C_i)^2$ where C_i^{expt} is the measured value of the capacitance at $V = V_i$ and C_i is the value of capacitance obtained numerically, n being the number of data points for a particular temperature [32]. K_{11} is related to the Freedericksz threshold voltage by: $V_{th} \propto \sqrt{K_{11}/\Delta\varepsilon}$; and from table 1, the values of $K_{11}/\Delta\varepsilon$ are 3.23, 3.10 and 1.51 for NLC, blend-1 and blend-2, respectively. It is clear that, as a consequence of decrease in $K_{11}/\Delta\varepsilon$, threshold voltage decreases successively. Although for blend-1 this decrease is only ∼2.1% but for blend-2 it is ∼31.5%, which is an excellent improvement for application to display devices. Low power

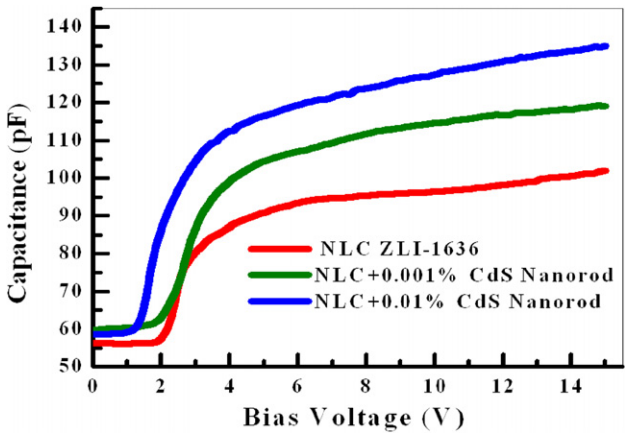

Figure 4. Graph showing the change in capacitance with applied voltage for all the samples. The blends show greater values of capacitance at the same applied voltage indicating higher dielectric anisotropy.

Table 1. Different physical parameters for pure NLC and blend; the frequency of the measuring signal was 5 kHz.

Parameters	$C_{\parallel}$ (pF)	$C_{\perp}$ (pF)	$\varepsilon_{\parallel}$	$\varepsilon_{\perp}$	$\Delta\varepsilon$	V_{th} (cal)	κ (cal)	K_{11} (pN)	K_{33}(pN)	K_{33}/K_{11}
ZLI-1636	115.03	56.3	8.044	3.93	4.11	1.90	0.5	13.29	19.94	1.5
ZLI-1636 +0.001% CdS	127.97	59.8	8.83	4.13	4.70	1.86	1.19	14.59	31.95	2.18
ZLI-1636 +0.01% CdS	149.91	58.6	10.41	4.04	6.37	1.30	1.65	9.64	25.54	2.64

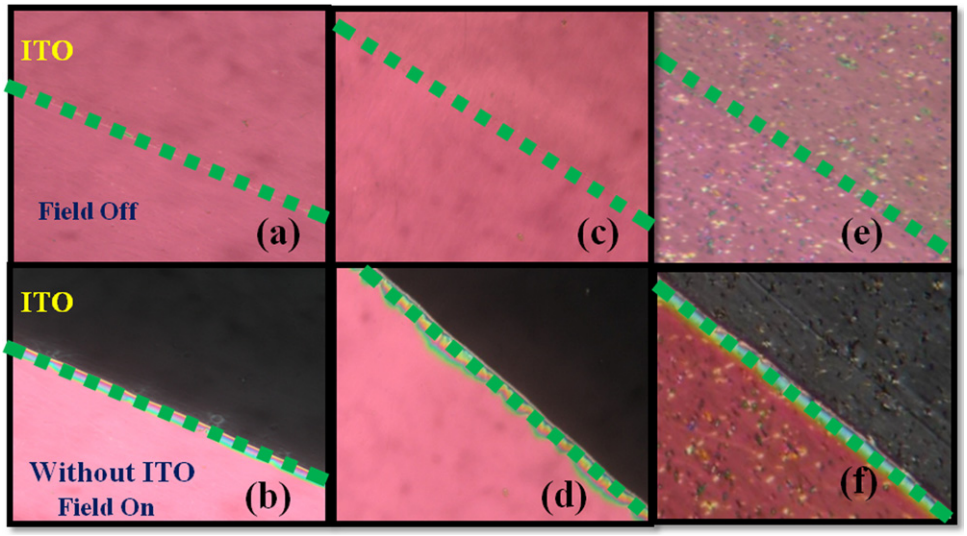

Figure 5. Polarizing optical microscopy (POM) textures of the cells, where upper portion of the dotted line is the ITO-coated portion and lower portions are without the ITO-coated portion. The first row is the texture without an electric field whereas the second row is the electrically addressed portion. (*a*)–(*b*) pure NLC; (*c*)–(*d*) 00.001% CdS-doped (blend-1) and (*e*)–(*f*) 0.01% CdS-doped hybrid system (blend-2). In other words textures (*a*), (*c*) and (*e*) are the planar aligned textures on the ITO-coated and rubbed portions. On the other hand (*b*), (*d*) and (*f*) shows that due to field addressing only the ITO-coated portion becomes homeotropic and gets black.

consumption is one of the most desirable goals for display devices and one way to achieve this is by decreasing the threshold voltage. Elastic constants increase dramatically for both blends. This indicates that anchoring interaction between NLCs and nanorods makes a vital role in changing the dielectric properties and elastic constants. Nevertheless, the dipole moment of the CdS nanorods (as ethylenediamine has a net dipole moment of 1.8 D) may also play a vital role. Anchoring interaction between nanorods and NLCs could be of three types, depending on the dimensionless parameter $\mu = R/d_{\text{e}}$ [33–35], where R is the radius and $d_{\text{e}} = K/W$ is the surface extrapolation length and K is the average Frank elastic constant [1]. When $\mu \ll 1$, i.e. $R \ll d_{\text{e}}$, it is a weak anchoring and cannot produce any large deformation in the surrounding nematic matrix. Secondly, when $\mu > 1$, i.e. $R > d_{\text{e}}$, the nanorod also cannot produce deformation in the surrounding appreciably and is commonly called intermediate anchoring. Finally, when $\mu \gg 1$, i.e. $R \gg d_{\text{e}}$, it is called strong anchoring and tropological singularities result. For our case $K \approx 10 \times 10^{-12}$ N (calculated value from table 1); and we have taken anchoring energy $W \approx 10^{-6}$ J m^{-2}, which is typical for NLCs. We found moderately strong anchoring in our system, which means anchoring interaction plays a dominant role in the changes in splay and bend elastic constants.

The increment in the bend elastic constant, K_{33}, might be due to the increase in the elasticity in the lateral dimension [36]. The ratio K_{33}/K_{11} also increases as shown in table 1. The development of materials with tailored values of the ratio K_{33}/K_{11} was historically driven by the need for sharp switching thresholds in order to optimize the contrast ratio in multiplexed twisted nematic and supertwisted nematic displays [37]. Increase in $\Delta\varepsilon$, K_{33}/K_{11} also has applications in higher Kerr effect [38]. Figure 5 shows the POM images of the three cells. The upper portion of the dotted line is the ITO-coated portion, whereas the lower portions are without the ITO-coated portion. The first row is the textures without an electric field addressing whereas the second row is the electrically addressed portion. (*a*) and (*b*) are for pure NLC; (*c*) and (*d*) for 00.001% CdS-doped (blend-1), and (*e*) and (*f*) for 0.01% CdS-doped hybrid system (blend-2). In other words texture (*a*), (*c*) and (*e*) are the planar aligned textures on the ITO-coated and rubbed portions. On the other hand, (*b*), (*d*) and (*f*) show that due to field addressing only the ITO-coated portion becomes homeotropic and gets black. It is also evident from the figure that the black state represents good, defect-free and monodomain textures, achieved (blend-1) for low concentration of CdS, whereas for higher content (blend-2) of CdS a few defects arise due to mutual interaction between nanorods. For low CdS content, defect-free textures may help one to attain a good contrast ratio. We have estimated blackness by measuring the luminance (a.u.) under the same light condition and in the homeotropic configuration of the three samples and interestingly we have observed that blend-1 has the minimum dark level. Nevertheless, for blend-2 darkness is not perfect but it could be improved by capping

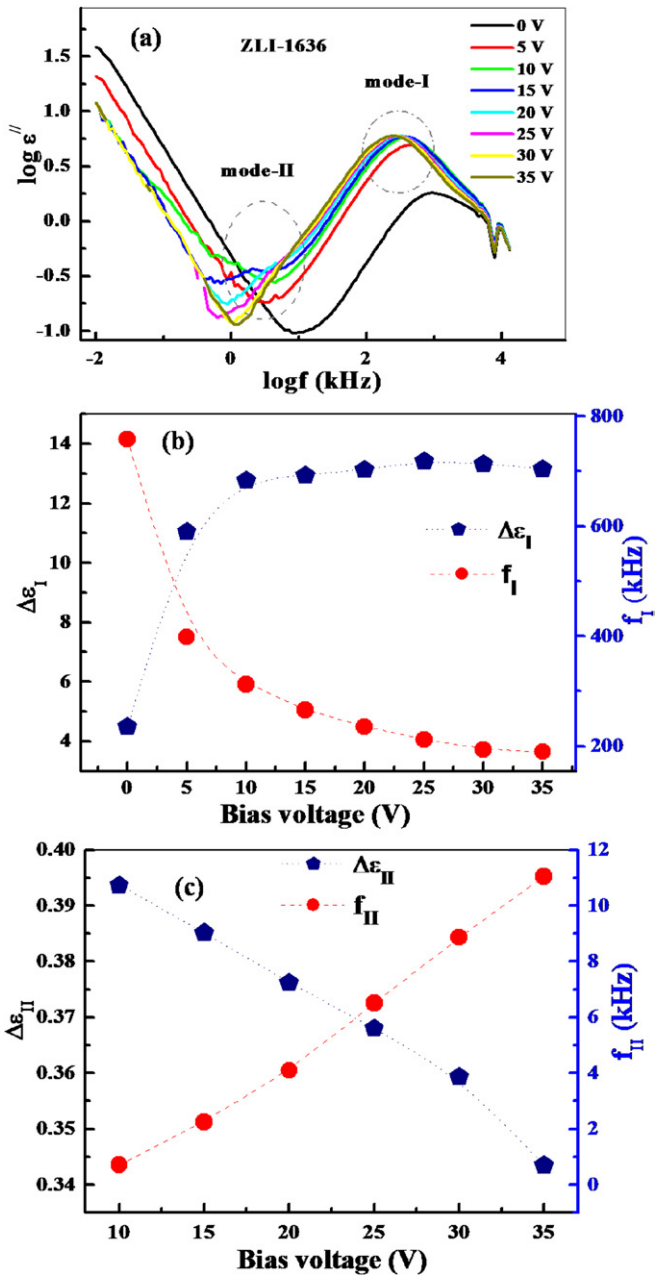

Figure 6. (*a*) Dielectric loss versus frequency in the logarithmic scale for NLC; (*b*) dielectric strength and relaxation frequency plotted against bias voltages for mode-I; (*c*) dielectric strength and relaxation frequency for mode-II.

and/or optimizing the sonication time so that we can screen the mutual interaction between nanorods.

Interpretation of the dielectric relaxation spectra was made with strong emphasis on a given absorption band to a particular mode of the molecular movement. Figure 6(*a*) shows the imaginary part of the dielectric constant (ε'') versus frequency in the logarithmic scale for the NLC blend at different bias voltages. Two relaxation processes named mode-I and mode-II arose. The dielectric strength ($\Delta\varepsilon$) and relaxation frequency (f_R) of these two modes are plotted in figure 6(*b*). At 0 V bias, the cell is in planar geometry and only one mode arises with relaxation frequency 757.88 kHz, and the dielectric strength is 4.48. In this planar geometry, the electric field acts perpendicular to the nematic director and this high-frequency process might be related to the tumbling motion of the molecules, i.e. the fluctuations of the dipole moment along the molecular long axis, around the local director [39, 40]. When the bias voltage is increased from 0 V up to ∼10 V, the NLC undergoes a Freedrezicks transition, then homeotropic configuration of molecules is achieved and molecular rotation around the short axis (180° rotation) becomes easier and, consequently, f_R is decreased. The dielectric relaxation mode in this homeotropic configuration is named mode-I. Mode-II arises at 10 V bias, i.e. in the homeotropic configuration in the lower frequency side. The activation energy for this mode-II was calculated, and its numerical value is 8.94 kJ mol^{-1}. The pre-exponential factor for the mode-II relaxation process is $\tau_0 = 1.58 \times 10^{-3}$ s, which is high compared with the Debye relaxation time $\tau_D = 1.76 \times 10^{-13}$ s [41]. This low-frequency mode-II is due to the influence of the ion drift [42].

Figure 7(*a*) shows the dielectric loss spectra of blend-I with different bias voltages. Here three dielectric relaxation processes are marked. At 0 V bias two dielectrically active modes are evolved, denoted as mode-I (blend-1) and mode-III (blend-1). Mode-I (blend-1) arises from the low-frequency side and it shifts towards the higher frequency side with higher bias voltages. The variation of dielectric strength and relaxation frequency of mode-I with a bias electric field is shown in figure 7(*b*). Gradual increases in $\Delta\varepsilon$ indicate that the LC alignment along the electric field lines becomes more ideal. This mode-I at higher voltages is due to rotation of the molecules around the short molecular axis. This type of bias-dependent $\Delta\varepsilon$ was reported earlier for E7 [43]. Figure 7(*c*) is the $\Delta\varepsilon$ and f_R of mode-II for blend-1. Mode-II first arose at ∼10 V bias like NLC. Figure 7(*d*) shows the $\Delta\varepsilon$ and f_R plot of mode-III. At 0 V bias, mode-III is the tumbling motion of the molecules, which is interesting because $\Delta\varepsilon$ is decreased and f_R is increased with respect to NLC at 0 V. Decreases in $\Delta\varepsilon$ with respect to NLC at 0 V might be due to the confinement of the NLCs by the CdS nanorods in this cell geometry [44] and as a consequence the relaxation frequency is increased. This also reflects the strong interaction of the NLC with nanorods. At 0 V bias the dielectric strength of mode-III is ∼1.5 and f_R is ∼5300 kHz. When $V > 10$ V the cell is perfectly black indicating homeotropic configuration of the blends. At this configuration mode-III has $\Delta\varepsilon \sim 2.5$, and the relaxation frequency shifts towards the lower frequency side, ∼3000 kHz. The origin of this mode-III may possibly be the fact that the molecules stick to the surface of the nanorods temporarily in an arbitrary manner. When the bias voltage increases the molecules gain electrical field energy to overcome the potential energy barrier induced by the surface anchoring, and the number of dipoles with a component of dipole moment vector along the parallel direction to the electric field increases, and as a consequence $\Delta\varepsilon$ increases. The existence of such surface layers with retarded molecular dynamics is well established on E7-hydroxypropylcellulose substrates and also by other authors [45–47]. Mode-II of blend-1 originates due to the same ion drift mechanism as in the case of NLC.

Figure 8(*a*) is the dielectric loss versus frequency curve at different bias voltages for blend-2. Three relaxation processes

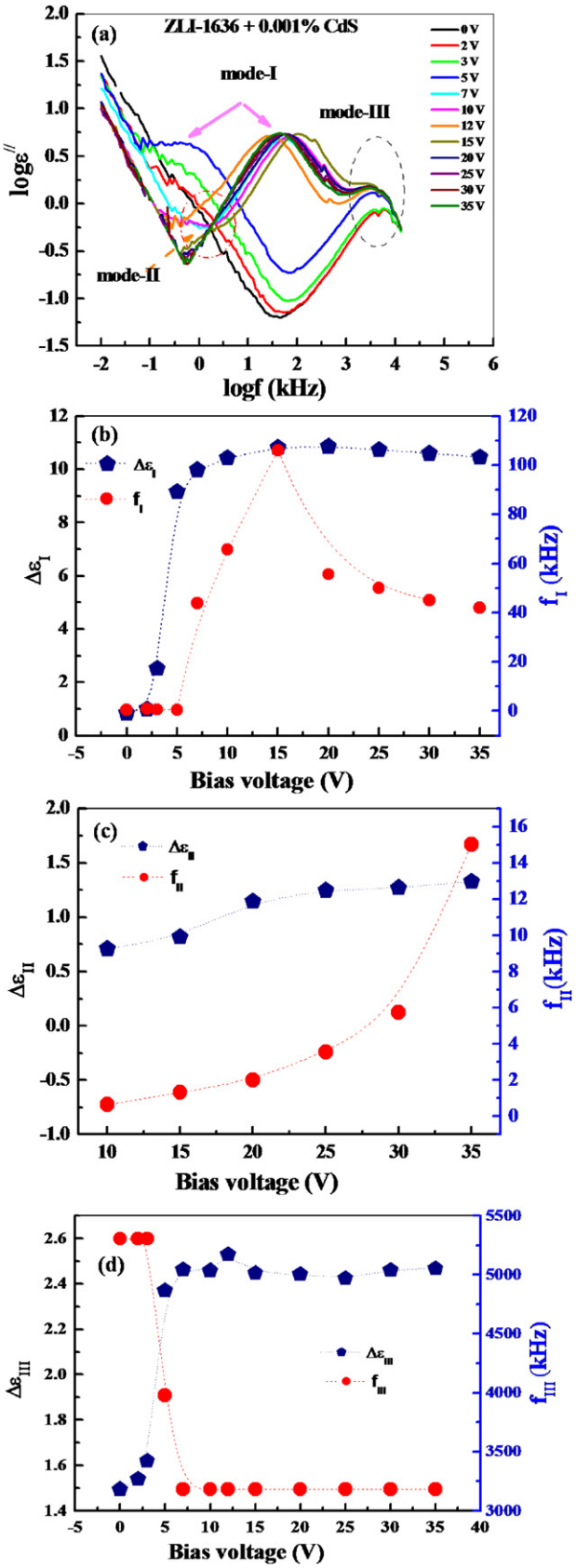

Figure 7. (*a*) Dielectric loss versus frequency in the logarithmic scale for blend-1; (*b*) dielectric strength and relaxation frequency plotted against bias voltages for mode-I; (*c*) dielectric strength and relaxation frequency for mode-II; (*d*) dielectric strength and relaxation frequency for mode-III.

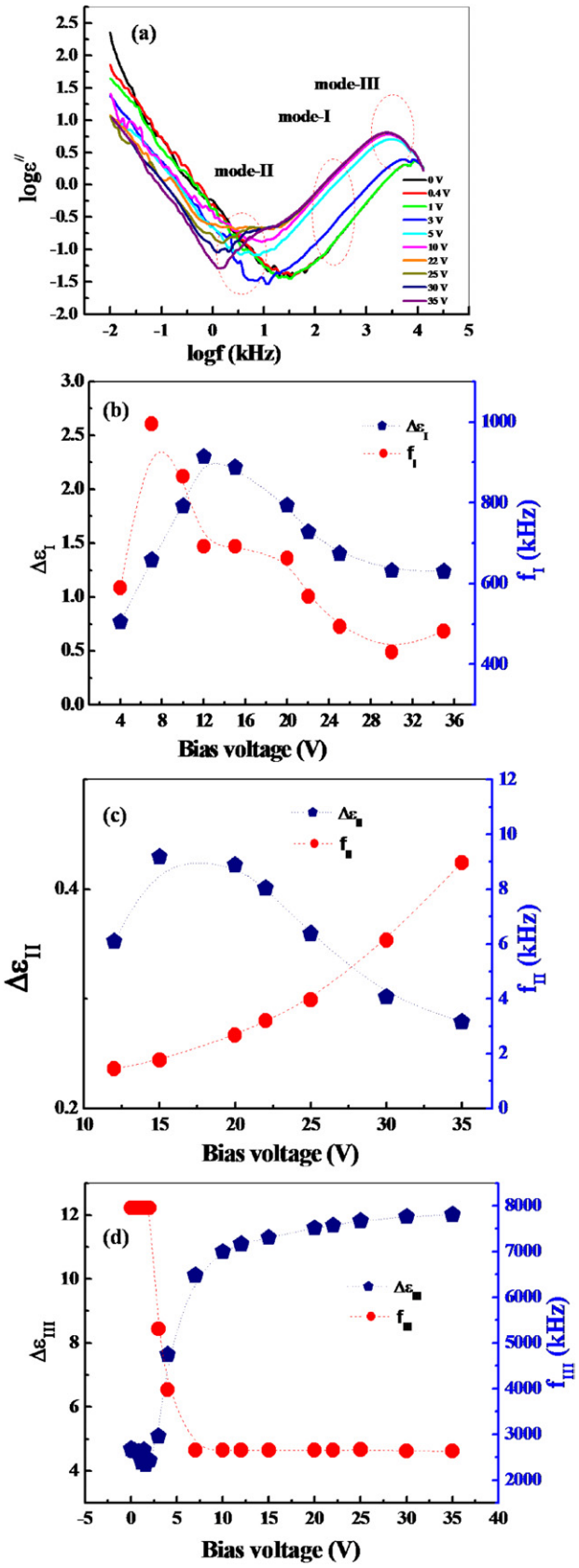

Figure 8. (*a*) Dielectric loss versus frequency in the logarithmic scale for blend-2; (*b*) dielectric strength and relaxation frequency plotted against bias voltages for mode-I; (*c*) dielectric strength and relaxation frequency for mode-II; (*d*) dielectric strength and relaxation frequency for mode-III.

are designated as mode-I, mode-II and mode-III. Figure 8(*b*) shows the variation of $\Delta\varepsilon$ and f_R for mode-I. This mode has an activation energy of 40 kJ mol^{-1} and is the molecular rotation around the short axis. $\Delta\varepsilon$ is decreased due to the confinement of the NLC by extra percentage of CdS nanorods. In figure 8(*c*), mode-II is due to the ion drift. Mode-II has $\Delta\varepsilon$ and f_R comparable to the NLC and blend-1. Figure 8(*d*) is the double Y-axis plot of mode-III and it shows the dielectric strength and relaxation frequency of this mode with bias voltage. The variation of relaxation frequency is similar to that of blend-1 (figure 7(*d*)) and $\Delta\varepsilon$ is higher than that of blend-1. A possible explanation could be that 0.01% CdS nanorods increase the number of nanorods per unit volume and also the number of dipoles adhered to CdS, and as a consequence $\Delta\varepsilon$ increases.

Finally, we can say that an increase in $\Delta\varepsilon$, as a consequence of the increase in long-range orientational order, is established (as $\Delta\varepsilon \propto S$: order parameter, [48]) in the blend. The increase in $\Delta\varepsilon$ is associated with the anchoring energy and anisotropic structures of CdS. The high miscibility for low CdS content in the composite makes good dark states and fewer topological defects during electric field addressing, which is clear from the texture study. For blend-1 NRs are readily miscible in the LC host matrix because of the ethylenediamine used and screening of the inter-rod van der Waals forces. CdS NRs composites may be exploited for low-threshold and high-contrast display devices.

4. Conclusion

Detailed dielectric study and analysis were made on pure nematic liquid crystal materials and two other blends composed of that nematic liquid crystal and ethylenediamine capped CdS nanorods in different ratios. The dielectric data reveal an additional relaxation process in the blends and that particular mode arises due to the presence of nanorods, which introduce some restriction on the neighbouring liquid crystal molecules. The threshold voltage for switching is lowered and the phenomenon is described from the C–V measurements. The ratio, K_{33}/K_{11}, is increased upon addition of nanorods in the LC mixture and this indicates the improvement of order parameter. From this phenomenon it can be concluded that further studies on materials can produce better blends and they can be used in real life display devices after proper investigations.

Acknowledgment

Some authors are grateful to the WCU program through MEST (R31-2008-000-20029-0) for financial support.

References

[1] Gennes P G de 1974 *The Physics of Liquid Crystals* (Oxford: Clarendon Press)
[2] Robbie K, Broer D J and Brett M J 1999 *Nature* **399** 764–66
[3] Grollau S, Abbott N L and Pablo J J de 2003 *Phys. Rev.* E **67** 051703
[4] Fukuda J, Yoneya M and Yokoyama H 2002 *Phys. Rev.* E **65** 041709
[5] Loudet C J, Barois P and Poulin P 2000 *Nature* **407** 611–3
[6] Andrienko D, Allen M P, Skacej G and Zumer S 2002 *Phys. Rev.* E **65** 041702
[7] Woltmann S J, Jay G D and Crawford G P 2007 *Nature Mater.* **6** 929–38
[8] Acharya S, Panda A B, Efrima S and Golan Y 2007 *Adv. Mater.* **19** 1105–8
[9] Acharya S, Patla I, Kost J, Efrima S and Golan Y 2006 *J. Am. Chem. Soc.* **128** 9294–5
[10] Pradhan N, Acharya S, Ariga K, Karan N S, Sarma D D, Wada Y, Efrima S and Golan Y 2010 *J. Am. Chem. Soc.* **132** 1212–3
[11] Acharya S, Sarma D D, Golan Y, Sengupta S and Ariga K 2009 *J. Am Chem. Soc.* **131** 11282–3
[12] Acharya S, Sarma D D, Jana N R and Pradhan N 2010 *J. Phys. Chem. Lett.* **1** 485–8
[13] Jana N R, Gearheart L A and Murphy C 2001 *J. Phys. Chem.* B **105** 4065–7
[14] Yada M, Yamamoto J and Yokoyama H 2004 *Phys. Rev. Lett.* **92** 185501-4
[15] Wu K J, Chu K C, Chao C Y and Chen Y F 2007 *Nano Lett.* **7** 1908–13
[16] Lapointe C, Hultgen A, Silevitch D M, Felton E J, Reich D H and Leheny R L 2004 *Science* **303** 652–5
[17] Koenig G M Jr, Meli M V, Park J S, de Pablo J J and Abbott N L 2007 *Chem. Mater.* **19** 1053–61
[18] Brochard F and de Gennes P G 1970 *J. Phys. (Paris)* **31** 691
[19] Rault J, Cladis P E and Burger J P 1970 *Phys. Lett.* A **32** 199–200
[20] Chen S-H and Amer N M 1983 *Phys. Rev. Lett.* **51** 2298–301
[21] Lapointe C P, Mason T G and Smalyukh I I 2009 *Science* **326** 1083–6
[22] Engström D, Trivedi R P, Persson M, Goksör M, Bertness K A and Smalyukh I I 2011 *Soft Matter* **7** 6304–12
[23] Kim P *et al* 2012 *Nano Lett.* **12** 527–33
[24] Senyuk B *et al* 2012 *Nano Lett.* **12** 955–63
[25] Dontabhaktuni J, Ravnik M and Žumer S 2012 *Soft Matter* **8** 1657–63
[26] Acharya S, Kundu S, Hill J P, Richards G J and Ariga K 2009 *Adv. Mater.* **21** 989–93
[27] Kundu S, Hill J, Richards G, Ariga K, Khan A H, Thupakula U and Acharya S 2010 *ACS Appl. Mater. Interfaces* **2** 2759–66
[28] Havriliak S and Negami S 1966 *J. Polym. Sci.* C **14** 99–117
[29] Morris S W, Muhoray P P and Balzarini D 1986 *Mol. Cryst. Liq. Cryst.* **139** 263–80
[30] Freedericksz V and Tsvetkov V 1934 *Phys. Z. Sowjetunion* **6** 490–504
[31] Gruler H, Scheffer T J and Meier G Z 1972 *Z. Naturf.* **27A** 966–76
[32] Das Gupta S, Chattopadhyay P and Roy S K 2001 *Phys. Rev.* E **63** 041703
[33] Burylov S V and Raikher Yu L 1994 *Phys. Rev.* E **50** 358
[34] Burylov S V and Raikher Yu L 1990 *Phys. Lett.* A **149** 279
[35] Popa-Nita V and Kralj S 2010 *J. Chem. Phys.* **132** 024902
[36] Sridevi S, Krishna Prasad S, Nair G G, D'Britto V and Prasad B L V 2010 *Appl. Phys. Lett.* **97** 151913
[37] Strömera J F, Raynes E P and C V Brown 2006 *Appl. Phys. Lett.* **88** 051915
[38] Choi S-W, Yamamoto S-I, Haseba, Higuchi H and Kikuchi H 2008 *Appl. Phys. Lett.* **92** 043119
[39] Viciosa M T, Nunes A M, Fernandes A, Almeida P L, Godinho M H and Dionsio M D 2002 *Liq. Cryst.* **29** 429–41
[40] Aliev F M, Nazario Z and Sinha G P 2002 *J. Non-Cryst. Solids* **305** 218–25

[41] Majumder T P, Meißner D and Schick C 2004 *Carbohydrate Polym.* **56** 361–6
[42] Mada H and Yamada H 1994 *Japan. J. Appl. Phys.* **33** 5886–7
[43] Vanboxtel M C W, Bbenhorst M W, Turnhout J V, Bastiaansen C W M and Broer D J 2003 *Liq. Cryst.* **30** 235–9
[44] Nayek P, Ghosh S, Karan S, Majumder T P and Roy S K 2008 *Appl. Phys. Lett.* **93** 112905
[45] Lippens D, Parneix J P and Chapoton A 1977 *J. Physique* **38** 1465–71
[46] Wacrenier J M, Druon C and Lippens D 1981 *Mol. Phys.* **43** 97–112
[47] Cramer Ch, Cramer Th, Arndt M, Kramer F, Naji L and Stanarius R 1997 *Mol. Cryst. Liq. Cryst.* **303** 209–17
[48] Bahadur B 1990 *Liquid Crystals Applications and Uses* vol 1 (Singapore: World Scientific) p 327 chapter 13